The Structure of L-Aspartate Ammonia-Lyase from *Escherichia coli*[†,‡]

Wuxian Shi,[§] Jennifer Dunbar,[§] Maithri M. K. Jayasekera,[||] Ronald E. Viola,[||] and Gregory K. Farber*[,§]

Department of Biochemistry and Molecular Biology, 108 Althouse Laboratory, The Pennsylvania State University, University Park, Pennsylvania 16802, and Department of Chemistry, University of Akron, 190 East Buchtel Common, Akron, Ohio 44325

Received February 27, 1997; Revised Manuscript Received May 22, 1997[⊗]

ABSTRACT: The X-ray crystal structure of L-aspartate ammonia-lyase has been determined to 2.8 Å resolution. The enzyme contains three domains, and each domain is composed almost completely of α helices. The central domain is composed of five long helices. In the tetramer, these five helices form a 20-helix cluster. Such clusters have also been seen in δ-crystallin and in fumarase. The active site of aspartase has been located in a region that contains side chains from three different subunits. The structure of the apoenzyme has made it possible to identify some of the residues that are involved in binding the substrate. These residues have been examined by site-directed mutagenesis, and their putative roles have been assigned [Jayasekera, M. M. K., Shi, W., Farber, G. K., & Viola, R. E. (1997) *Biochemistry 36*, 9145−9150].

Enzymes that remove a proton which is α to a carboxylate have intrigued enzymologists for many years. There are a number of enzymes which catalyze this reaction, and among the best studied of these enzymes are fumarase, enolase, aconitase, amino acid ammonia-lyases, and mandelate racemase. The reason that these enzymes have been studied so intensively is that the pK_a of the proton to be removed is quite high. For mandelate racemase, this pK_a has been measured to be 22 (Chiang et al., 1991), and this is typical of substrates for these enzymes.

Aspartate ammonia-lyase (aspartase)[1] catalyzes the deamination of aspartic acid to form fumarate and ammonia (Figure 1). For the enzyme to catalyze this reaction two challenges must be met: removal of a quite basic proton and stabilization of the resulting aci-carboxylate intermediate. It is now clear from structural studies that mandelate racemase stabilizes the resulting intermediate through the interaction of a magnesium ion (Landro et al., 1994). Aconitase uses a 4Fe-4S cluster to stabilize a similar intermediate (Beinert & Kennedy, 1993). However, most of the enzymes mentioned above do not require metal ions for catalysis, so alternative stabilization strategies must have developed.

We have initiated structural studies on the ammonia-lyase enzymes to try to uncover the structural basis for catalysis. Here we report the structure of aspartase from *Escherichia coli* to 2.8 Å. Aspartase is a tetramer in solution and also in the crystal. The active site of this enzyme has been identified by site-directed mutagenesis studies (Saribas et al., 1994; Jayasekera et al., 1997). The structure reveals that residues from three different subunits are located close to the active site, with the potential to be involved in catalysis.

EXPERIMENTAL PROCEDURES

Protein Purification and Crystallization. L-Aspartate ammonia-lyase was purified from a plasmid-containing strain of *E. coli* that overproduces aspartase to about 20% of the total soluble protein following the procedure described by Karsten et al. (1985). Aspartase was crystallized by using the microdialysis method at 21 °C. 20 μL of protein solution at a concentration of 10−13 mg/mL in 50 mM Tris-Hepes, pH 7.5, was dialyzed against roughly 200 mL of reservoir solution containing 0.1 M, Tris-HCl, pH 8.5, 26% polyethylene glycol with an average molecular weight of 3350, 0.30 M sodium acetate, and 4 mM dithiothreitol (Shi et al., 1993). Initially, 4 mM DTT was used to shift the equilibrium from monomer to tetramer in solution (Shi et al., 1993). However, it is possible to substitute 3−5 mM glucose in place of DTT in the crystallization buffer to get the same type of aspartase crystals. Crystals grown in the presence of glucose did not deteriorate like those grown in the presence of DTT. As a result, native diffraction data collected from a crystal grown in the crystallization buffer containing glucose instead of DTT was used for the molecular replacement and in all subsequent stages of the structure determination and refinement. Aspartase crystals usually appeared in three days and took a week to ten days to attain maximum size. The largest crystals were of maximum dimensions 1.5 mm × 0.5 mm × 0.4 mm, and typically were 0.6 mm × 0.3 mm × 0.3 mm. The morphology of the crystals varied from clean prisms to dendritic crystals. Aspartase crystals tend to grow in clusters, but single crystals could be separated from the clusters easily. These crystals exhibited the symmetry of space group $P2_12_12$ with $a = 153.5$ Å, $b = 146.2$ Å, $c = 103.2$ Å. Unit cell lengths were determined from precession photographs of the three principal zones and were confirmed during data reduction with the program DENZO (Gewirth, 1994). The crystals contain a tetramer in the asymmetric unit with a V_m of 2.77 Å^3/Da (Matthews, 1968) and a calculated solvent content of 56%.

[†] This work was supported by Grant DK 47838 from the National Institutes of Health to G.K.F. and R.E.V.

[‡] The coordinates have been deposited in the Brookhaven Protein Data Bank under the filename 1JSW.

* To whom correspondence should be sent. e-mail: farber@ewald.bmb.psu.edu.

[§] The Pennsylvania State University.

[||] University of Akron.

[⊗] Abstract published in *Advance ACS Abstracts,* July 15, 1997.

[1] Abbreviations: aspartase, L-aspartate ammonia-lyase; DTE, dithioerythritol; DTT, dithiothreitol; MPD, 2-methyl-2,4-pentanediol; NCS, noncrystallographic symmetry.

S0006-2960(97)00451-0 CCC: $14.00

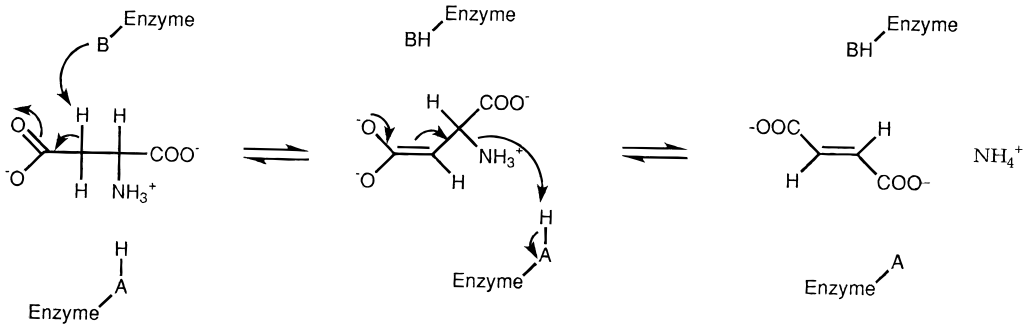

FIGURE 1: Chemical mechanism of aspartase. Aspartase catalyzes the formation of fumarate and ammonia from aspartic acid. There is still some uncertainty about the protonation state of the leaving group (see Discussion). After the products dissociate, a final enzyme isomerization step is necessary to return aspartase to the proper protonation state.

Table 1: Data Collection Statistics for Aspartase[a]

unit cell (Å)			resolution	no. of	unique	%		
a	*b*	*c*	(Å)	reflcns	reflcns	complete	$I/\sigma(I)$	R_{sym}[b]
153.53	146.22	103.23	2.8	156675	57964	80.3	10.8	0.076

[a] Space group $P2_12_12$; wavelength (Cu Kα) = 1.5418 Å. [b] $R_{sym} = \sum|I_{obs} - \langle I\rangle|/\sum\langle I\rangle$, where I_{obs} and $\langle I\rangle$ are the observed intensity of a single reflection and the average intensity of all measurements of a reflection and its Freidel mate, respectively.

Data Collection and Processing. Aspartase X-ray diffraction data was collected on flash frozen crystals using an R-axis II area detector and a Rigaku rotating anode X-ray generator operating at 100 mA, 50 KV. Radiation from the copper anode was monochromatized using a graphite crystal, and a 0.3 mm collimator was used for the data collection. Data collection was performed at −178 °C. Aspartase crystals were soaked in a cryoprotection buffer containing 1 M glucose, 4% isopropanol, and 1% MPD for at least 30 min before the flash-freezing to prevent ice formation in the crystal lattice. Indexing, integration, reduction, and scaling of the data were carried out using the program DENZO (Gewirth, 1994). A single crystal was needed for a complete data set. The native data set used for the molecular replacement and structure refinement steps had an overall 80.3% completeness to 2.8 Å resolution and an *R*-factor on symmetry-equivalent reflections (R_{sym}) of 7.6%. Data collection statistics are presented in Table 1. In the 3.02−2.80 Å resolution range, 67% of the unique reflections have $I \geq \sigma(I)$.

Molecular Replacement. The structure of aspartase from *E. coli* was solved by molecular replacement using the AMoRe software package (Navaza, 1994). Coordinates of fumarate hydratase (EC 4.2.1.2) from *E. coli* were used as the search model. The model was generously provided by Professor Len Banaszak. Aspartase and fumarase from *E. coli* have only 188 identical residues out of a possible total of 466. This relatively low sequence identity made molecular replacement difficult. All side chains in the model that are known from sequence alignment to differ from aspartase were trimmed to alanine. Fumarase crystallized in space group *C*2 with only two subunits of the tetramer in the asymmetric unit (Weaver et al., 1995). Coordinates of the other two subunits of the tetramer were generated by applying a crystallographic 2-fold axis. A fumarase molecule consists of three consecutive domains. The second domain which is the largest (250 residues) and most conserved domain in the aspartase−fumarase structural family is made up of five long, almost parallel helices, ranging from 25 to 38 residues in length. Because of the five-helix bundle structure in the central domain, the fumarase monomer has a very elongated shape with the longest dimension of about 100 Å and the other two dimensions of only 30−40 Å (Banaszak & Weaver, 1996).

The elongated monomer made choosing the model and integration radius for the Patterson function superposition very difficult. The first molecular replacement attempt used a monomer as the search model. The rotation function search gave six potential solutions which were separated from the other solutions when calculated with the various integration radii from 30−50 Å in 5 Å increments. A translation function was then calculated using the top 50 rotation function solutions. Unfortunately, this translation function gave no solutions with a clear separation in either the correlation coefficient or the *R*-factor. Use of either a monomer without the less conserved third domain or a dimer as the search model yielded equally unsatisfactory results in the translation function search.

Using a tetramer of only domain 2 as a search model yielded clear, convincing solutions in both the rotation and translation function searches. The domain 2 tetramer model has two advantages. In addition to the fact that this model provides close to half of the information in the asymmetric unit, the five-helix bundle of the second domain interacts to produce a central core of twenty nearly parallel α-helices in the tetrameric form of fumarase and the 20-helix bundle structure has a roughly spherical shape. This makes choosing an integration radius for Patterson function calculations relatively easy. For the rotation function only Patterson densities inside a spherical shell of inner and outer radii of 3 and 40 Å, respectively, were used in the Patterson map superposition. The five highest independent peaks in the cross rotation function map, calculated from X-ray data between 10.0 and 4.0 Å resolution, are listed in Table 2. A large separation was observed between the highest and next highest peaks. The top solution was assumed to represent the orientation of the tetramer in the asymmetric unit. The location of the tetramer was then determined by the corresponding translation function calculation. A moderate separation was observed in the correlation coefficient between the best and second best solutions in the translation map for the orientation (Table 2) while no separation was

Table 2: Molecular Replacement Calculations

A. Cross Rotation Function[a]				
RF peak no.	α	β	γ	peak height
1	117.89	70.61	33.89	19.0
2	27.90	70.98	146.7	13.2
3	106.38	90.00	90.61	12.4
4	72.61	27.05	91.57	12.2
5	84.85	68.02	216.84	11.8

B. Translation Function[b]				
rotation solution	*x*	*y*	*z*	correlation coefficient
117.89, 70.61, 33.89	0.4002	0.2911	0.2999	25.6
	0.4471	0.4625	0.1680	24.2
	0.4468	0.3934	0.1674	24.1
	0.4617	0.4960	0.1419	24.0
	0.4683	0.4283	0.1486	23.9

[a] Diffraction data resolution, 10−4 Å; search interval, 1.0°. [b] Diffraction data resolution, 10−4 Å.

observed in the translation search with incorrect orientations or with several other models that had been tried.

Electron Density Map Improvement. The initial aspartase model was generated by applying the molecular replacement solution to the whole fumarase tetramer. The model was subjected to 200 steps of rigid body refinement using XPLOR (Brünger, 1992). Each domain was defined as a rigid group, so a total of twelve rigid groups were defined in the aspartase tetramer. All movement had converged after 200 steps of refinement. The movements between subunits were rather large, as were the motions between domains in each subunit. However, even with the large movement during the rigid body refinement the aspartase monomers were still related by three strict 2-fold axes which are perpendicular to each other. The *R*-factor dropped from 53.3% to 47.9%, and the free *R*-factor was also reduced to 48.7% during the 200 steps of rigid body refinement. A $2F_o-F_c$ map was generated from the refined model. The connectivity of the electron density was good in most regions. We were convinced that the model was correct since there was obvious density at the places where the missing side chains should be located.

Solvent flattening (Wang, 1985) was used to further improve the density map using the program DM in the CCP4 package (Collaborative Computational Project, 1994). The solvent content was set conservatively to 0.40 to prevent the truncation of protein density. Phases were extended from 4.5 Å to the highest resolution of the data set in fourteen cycles. The resulting map was then subjected to 10 cycles of noncrystallographic (NCS) averaging. The program RAVE was used for the averaging, and the mask was generated by using the program MAMA (Kleywegt & Jones, 1993). The correlation coefficients of the B, C, and D molecules relating to the A molecule started at 40%−45% and reached over 80% in the last cycle.

Model Building and Structure Refinement. The program O (Jones et al., 1991) was used to view the structure and build the missing side chains. Only the D molecule was rebuilt, and the other three molecules were generated using the matrices that relate the tetramer after the rigid body refinement step. The complete aspartase tetramer with all the missing side chains included was submitted to a cycle of simulated annealing refinement with the NCS constraint option in XPLOR. In this and subsequent cycles of simulated annealing, the structure was heated to 2500 K and cooled in increments of 25 K. After each cooling step, 50 steps of molecular dynamics simulation were performed. The time step for each of these runs was 0.5 fs. A second cycle of simulated annealing, followed by 15 steps of grouped B-factor refinement, was carried out using a rather relaxed NCS restraint. During the relaxed NCS refinement, the structure was divided into two groups. Tight NCS restraints were placed on the helices in the structure (weight of 150 for main chain and 75 for side chain) while only loose restraints were used for the rest of the model (weight of 10 for main chain and 5 for side chain).

Table 3: Refinement Statistics

resolution range (Å)	10.0−2.8
no. of reflcns	43803 (75.6% complete)
B-factors (mean) (Å^2)	
7164 main-chain atoms	24.30
6507 side-chain atoms	25.15
69 water molecules	18.55
2 glucose molecules	43.77
1 acetate molecule	31.05
R_{free}	0.371
R_{cryst}	0.216
rms deviations from ideal values	
bonds (Å)	0.010
angles (deg)	1.63
dihedrals (deg)	22.4
impropers (deg)	1.51

Residues 1−459 had been used in each of the monomers for refinement up to this point. The disorder in the electron density at both the N- and C-termini of monomer C precluded any reliable placement of the protein structure in these regions. As a result, monomer C was only modeled from residues 5−417. Three additional cycles of rebuilding into $2F_o-F_c$ maps followed by positional and grouped *B*-factor refinement were performed. Simulated annealing was conducted in all but the final round of refinement. Gln 460 was added to monomer B in the rebuilding process because of the appearance of compelling density beyond Val 459.

During rebuilding two β-D-glucose molecules, one acetate, and 69 waters were added to the model. The glucose structure of Chu and Jeffrey (1968) was used as a model for the glucose. Refinement parameters for acetate were derived from a glutamic acid residue. Nonprotein molecules were added to regions of convincing density within reasonable distances of potential hydrogen bonding groups on the protein. The occupancy was set at 1.0 and the group *B*-factors were left unrestrained during refinement for all added molecules. The final model had an R_{cryst} of 0.216 and an R_{free} of 0.371. Results from the crystallographic refinement appear in Table 3.

RMSD calculations and superpositions of the subunits were performed using the CCP4 suite of programs.

RESULTS

Quality of the Refined Structure. The final $2F_o-F_c$ electron density is continuous and well defined for most of the main-chain atoms at the 1σ contour level (Figure 3). No convincing density was seen for residues 461−478 of aspartase in any of the monomers. The majority of the third domain of monomer C was also disordered. Monomers A, B, and D have good crystal packing interactions between their third domains and symmetry-related molecules, but the

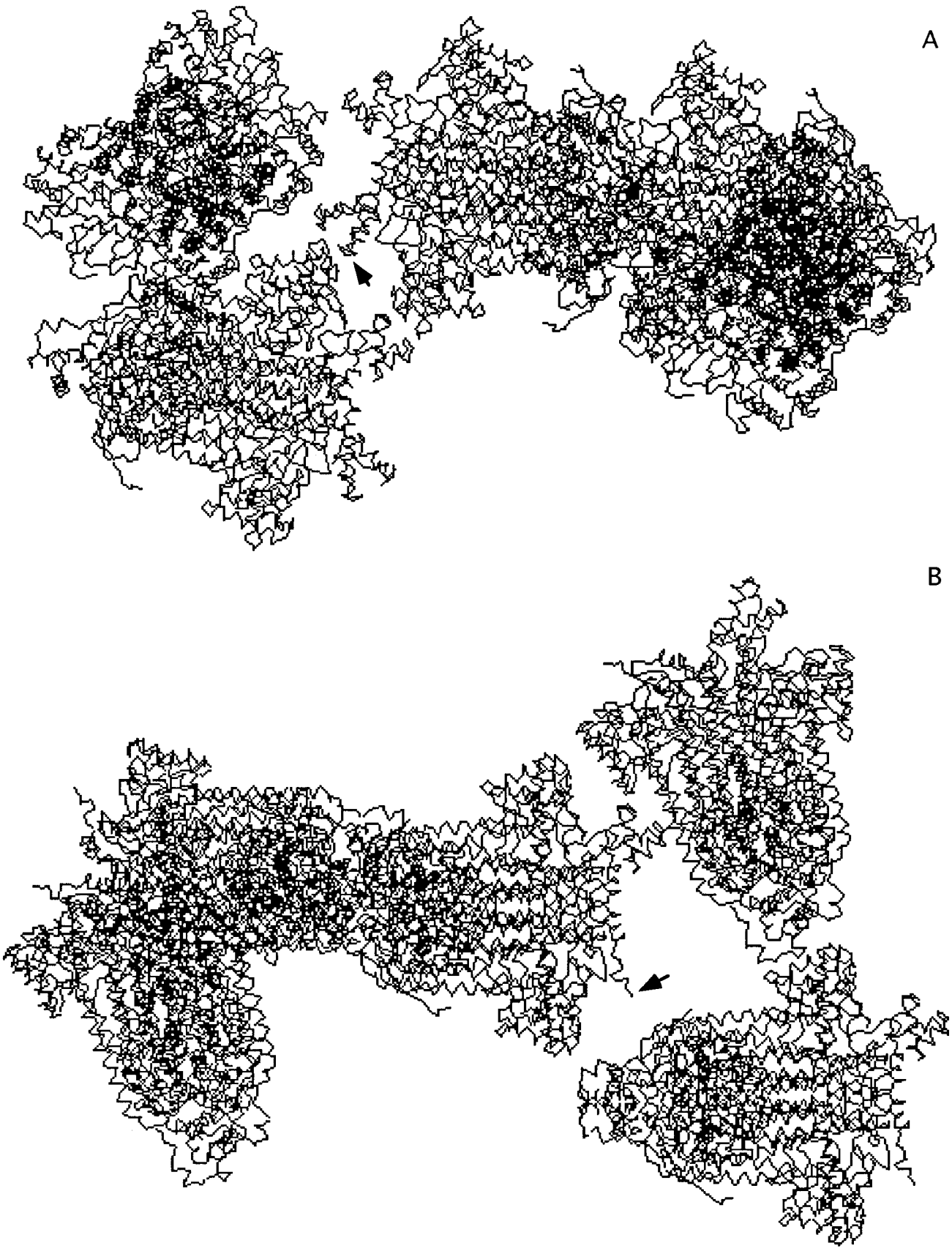

FIGURE 2: Cα backbone trace representing the intermolecular packing in the aspartase crystal near the third domain of monomer B (top figure) and monomer C (bottom figure). The symmetry-related molecules in each figure were generated by using a 20 Å sphere around residue 417. The arrow points to residue 417 in both cases. The lack of crystal packing interactions allows for flexibility and disorder in the third domain of monomer C. The tighter crystal packing near the third domain in monomer B reduces this flexibility.

third domain of monomer C is surrounded by a solvent channel, allowing for greater movement and disorder (Figure 2). Portions of 20 residues (1−5, 85−88, 237−238, 242, 269−273, 323−324, and 327) have weak density in all of

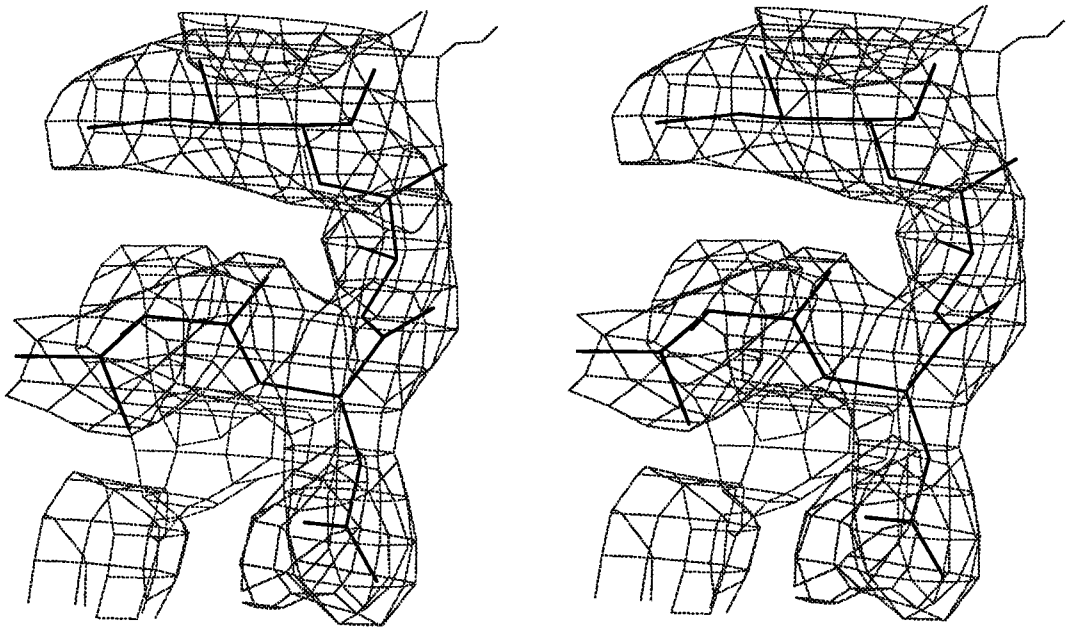

FIGURE 3: Stereoview of typical electron density for residues 164−167 of monomer A. The contour level is 1.1σ in this $2F_o-F_c$ map.

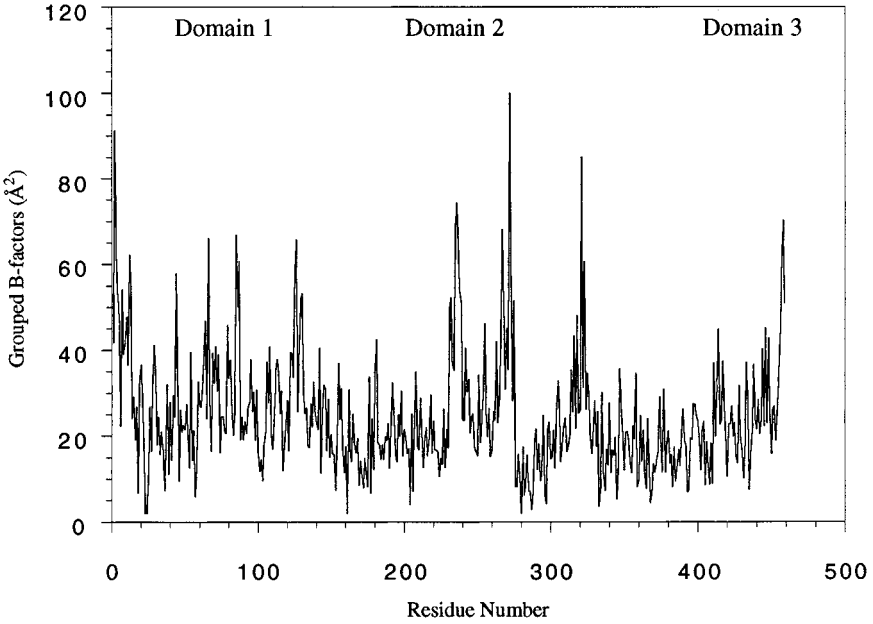

FIGURE 4: Grouped main-chain *B*-factor *versus* residue number for monomer A of the aspartase structure. Regions with the highest grouped *B*-factors are in the loop structures (see text).

the monomers. These portions of the structure fall within the flexible loops of the protein. Figure 4 is a plot of the grouped *B*-factor of the main-chain atoms *versus* residue number for a representative monomer. Residues in the disordered regions consistently have the highest grouped *B*-factors.

Figure 5 shows the Ramachandran plot for monomer D of aspartase. Of the 1581 non-glycine, non-proline residues modeled, 22 have main-chain ϕ,ψ dihedral angles in the disallowed regions of the Ramachandran plot as defined in PROCHECK (Laskowski et al., 1993). The residues in the disallowed regions are as follows: A monomer, Ala 232, Ala 270, Val 328; B monomer, Ser 2, Ala 19, Glu 46, Phe 47, Leu 192, Asp 266, Glu 269, Ala 270, Val 459; C monomer, Glu 46, Glu 269, Asp 273, Arg 306, Leu 359; D monomer-, Asn 86, Asn 133, Thr 233, Lys 243, Asp 273. All of these residues, with the exception of Ser 2 and Val 459 in B, are in loops or tight turns in the structure. A consistently problematic segment involves residues 266−273. The density in this region does not account for all residues present, thereby causing some strain on the model as Thr 271 and Ser 272 loop out of the density. The model and density match very well both immediately preceding and following this section, however, and several attempts to rebuild these residues and improve their geometry failed.

The R_{cryst} of 0.216 and R_{free} of 0.371 are within acceptable ranges for a structure of this resolution (Kleywegt & Brünger, 1996). Based on the fact that three positional parameters were fit for each of the 13 768 heavy atoms in the protein, that two thermal factors were used for each of 1787 residues, and that a single thermal factor was used for the 72 solvent molecules, 44 950 parameters were fit in the structure. Only 43 803 reflections were used in the refinement (Table 3). The structure is therefore slightly underdetermined in the

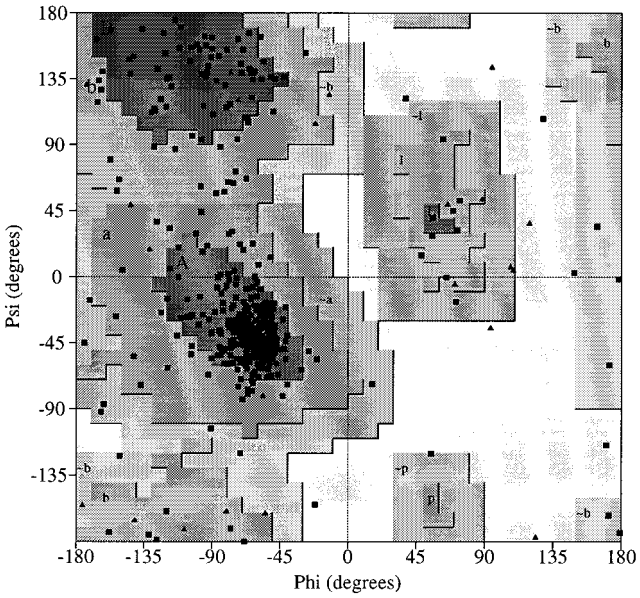

FIGURE 5: Ramachandran plot for the final refined coordinates of monomer D. Glycines are shown as triangles, and non-glycine residues are shown as squares. Five of the non-glycine, non-proline residues are in the disallowed regions of the plot. Drawn with PROCHECK (Laskowski et al., 1993).

absence of any additional geometric constraints placed on the model. This underdetermination contributes to the significant, but acceptable, difference between R_{cryst} and R_{free} (Kleywegt & Brünger, 1996). It would have been possible to improve the ratio of parameters to reflections by forcing all four monomers to obey strict noncrystallographic symmetry. However, the difference in electron density in the C monomer after a examining variety of different NCS weighting schemes compelled us to abandon this approach.

Description of the Structure. The polypeptide fold of the aspartase tetramer is shown in Figure 6 and that of the monomer is shown in Figure 7. Table 4 lists the secondary structural elements in aspartase as defined by DSSP (Kabsch & Sander, 1983). Each monomer of aspartase is composed of three domains and has approximate dimensions of 40 Å × 40 Å × 110 Å. The N-terminal domain is composed of residues 1−141. It consists of a short, two-stranded antiparallel β-sheet followed by five helices. Helices 1 and 4 are antiparallel to each other. Similarly, helices 2 and 3 are antiparallel to each other and together are oriented almost perpendicularly to the helix 1/4 pair. Helix 5 is a short stretch of five residues right at the end of this domain. It has a combination of α and π helix character. DSSP lists it as a π helix for monomers A and D, an α helix for monomer C, and a hydrogen-bonded turn for monomer B. In all four monomers, the majority of the residues form hydrogen bonds of reasonable length from *i* to *i*+4 and *i*+5. The π *versus* α distinction in DSSP seems to pivot upon one hydrogen bond in each case which fits one classification but not the other. This π helix is close to the putative active site. A similar π helix was observed in fumarase (Banaszak & Weaver, 1996).

Domain 2 of aspartase, containing residues 142−396, has almost all α-helical structure. This domain contains more than half of the total residues and is the most conserved domain in the aspartase−fumarase structural family. The central core of the domain is made up of five helices: 6, 7, 9, 10, and 11. These helices are all slightly bent and are nearly parallel to each other. They range from 25 to 38 residues in length and make domain 2 very long (about 50 Å). Helices 6 and 7 are connected by an antiparallel β-structure. The relatively short helix 8 connects to helices

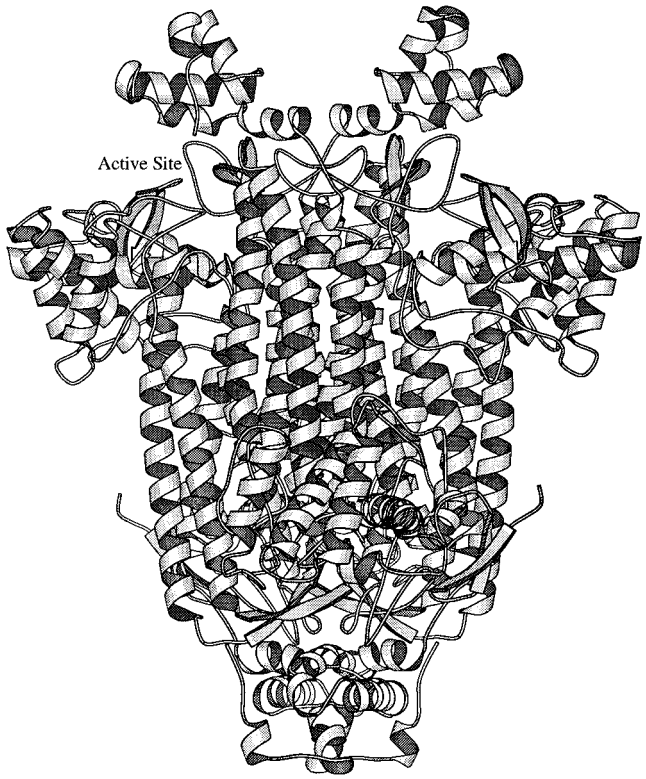

FIGURE 6: Molscript (Kraulis, 1991) diagram of the tetramer of aspartase. The helices, strands, and loops are shown as helical ribbons, arrows, and lines, respectively. One of the four active sites in the aspartase tetramer is labeled.

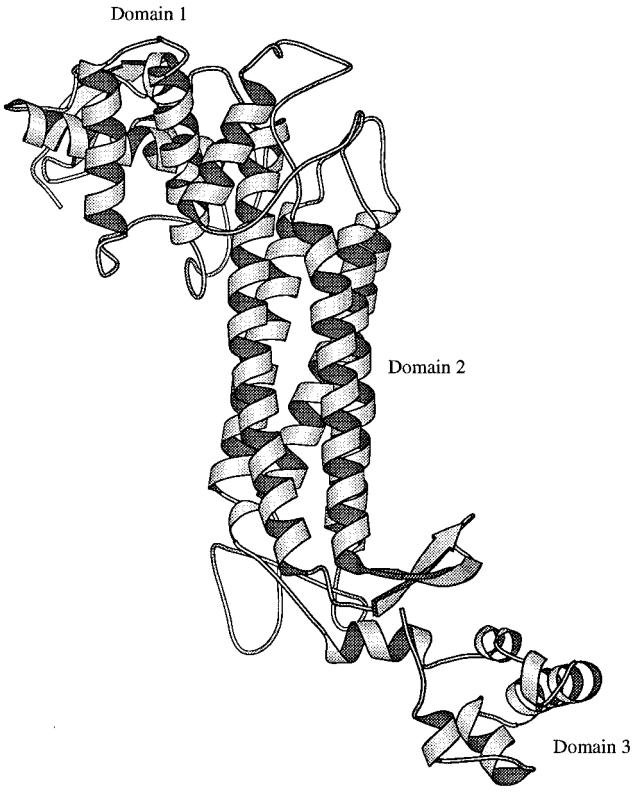

FIGURE 7: Molscript (Kraulis, 1991) diagram of an aspartase monomer. The elongated nature of the monomer is evident.

Table 4: Secondary Structural Elements of Aspartase[a]

domain 1				domain 2				domain 3	
α helices		β strands		α helices		β strands		α helices	
1	25−33	A	6−10	6	144−181	C	185−190	12	398−405
2	47−65	B	13−17	7	200−225	D	193−199	13[c]	411−417
3	70−83			8	245−257			14	421−432
4	104−122			9	277−301			15	438−445
5[b]	134−138			10	331−355			16	450−454
				11	365−389				

[a] Given the similarity of secondary structure among the monomers, residue listings are only given for monomer A. [b] Helix 5 has a mixture of α and π helix character. [c] Helix 13 exhibits 3_{10}-helix bonding patterns at its N-terminus.

Table 5: RMS Deviations (Å) for Cα Atoms among Monomers[a]

	B	C	D
A	0.796	0.717	0.960
B		0.771	0.982
C			0.754

[a] Calculated with the program LSQKAB in the CCP4 suite of programs.

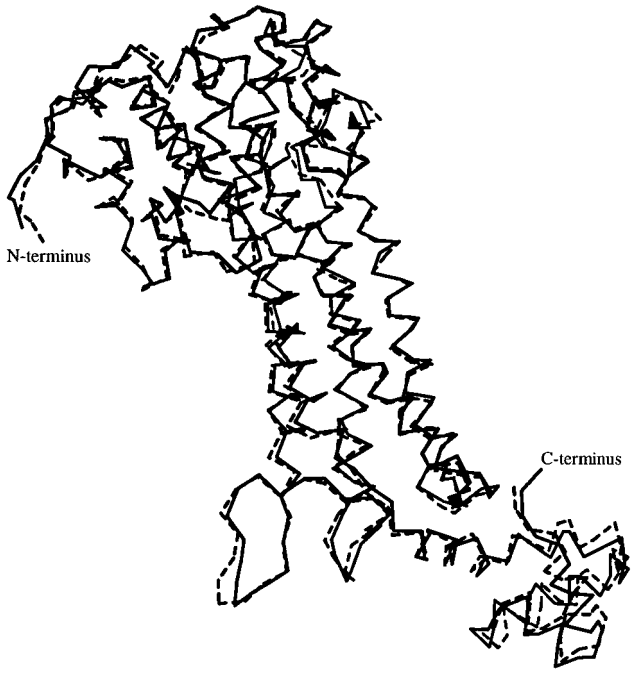

FIGURE 8: Superposition of the Cα trace of monomer B onto monomer D. Monomer B is shown with the solid line, and monomer D is represented by the dashed line. The major differences arise in the loop structures and in the relative orientation of domain 3 in B compared to D.

7 and 9 by two long loops, making this part of the structure very flexible. Helix 11 extends to Lys 389, but there is pseudohelical structure from Ile 391 to Gly 393. The five-helix bundle structure is arranged in the up-down-up-down-up topology common to all members of the aspartase−fumarase structural family (Weaver et al., 1995; Simpson et al., 1994).

The C-terminal domain includes residues 397−459 and is the smallest domain in the subunit. It has a similar arrangement to the amino terminal domain, consisting mainly of two helix−turn−helix motifs oriented approximately 90° relative to each other. Helices 13 and 14 form one helix−turn−helix motif, while helices 15 and 16 form the other. Helix 13 has 3_{10} character at its N-terminus and α-helix values toward its C-terminus.

The four subunits of aspartase are arranged with the point symmetry 222. There are three unique dimer interfaces in the tetrameric structure. These are analogous to the interfaces present in fumarase (Weaver et al., 1995), although the subunit pairing is different. The rms deviations for the Cα atoms of the four monomers are shown in Table 5. The elements of secondary structure superimpose well, but the positioning of the flexible loops can vary considerably from one monomer to the next. Figure 8 shows the superimposition of monomer B onto monomer D. In this worst case the major causes of deviation are the loop structures and the positioning of the carboxy terminal in B compared to that in D. The relative orientation of the three domains in molecule D is slightly altered from that found in subunit A, B, or C. Root mean square deviations were calculated for the Cα atoms of each domain of the monomers. In comparisons with monomer D, the rms deviation for the whole molecule is larger than that for any of the domains (data not shown). It is unclear whether this is physiologically relevant or simply a result of crystal packing.

Small Molecule Binding Sites. Figure 9 shows the final position of glucose 601A and glucose 601B. Both glucoses form hydrogen bonds with aspartase side chains. Oxygen O1 of glucose 601A forms hydrogen bonds with both Glu 388A Oε1 (2.95 Å) and Glu 388A Oε2 (2.56 Å). Water 511 forms a hydrogen bond with O4 (2.88 Å) on the other side of the glucose. Glucose 601B forms hydrogen bonds from O3 to Asp 165B Oδ1 (2.98 Å) and from O4 to Asp 165B Oδ2 (2.93 Å). Glucose 601B is positioned between two symmetry-related molecules, but no additional hydrogen bonds are formed. The binding of glucose to aspartase appears to be important since addition of glucose (or DTT) to the crystallization buffer is an essential step in obtaining diffraction quality crystals. Interestingly, neither DTE nor β-mercaptoethanol could substitute for DTT during crystallization (Shi, et al., 1993).

Acetate 701 is at a crystal packing interface, close to both Arg 445A Nη2 (3.92 Å) and Gly 123C O (3.19 Å) from a symmetry-related molecule. It is not involved in any hydrogen bonding interactions; however, away from the symmetry interface it is bordered by a solvent channel.

DISCUSSION

The proposed active site of aspartase has been located on the basis of sequence alignments of the fumarase superfamily and mutagenesis studies (Saribas et al., 1994), but the identity of the residues involved in catalysis has not been determined. The high substrate specificity of aspartase suggests that the enzyme must bind both the α- and β-carboxylate groups (Falzone et al., 1988). pH studies of the enzyme (Yoon et al., 1995) suggest that these binding residues must have a pK_a higher than 9. Either Lys or Arg are good candidates for these binding groups. In the vicinity of the active site, mutations at both Arg 29 (Jayasekera et al., 1997) and Lys 327 (Saribas et al., 1994) have an effect on substrate binding.

The identity of the catalytic residues is still uncertain from the structure of the apoenzyme. It is known that the enzymatic acid has a pK_a in the range 7.2−7.6 (with no magnesium present) and that the base has a pK_a in the range

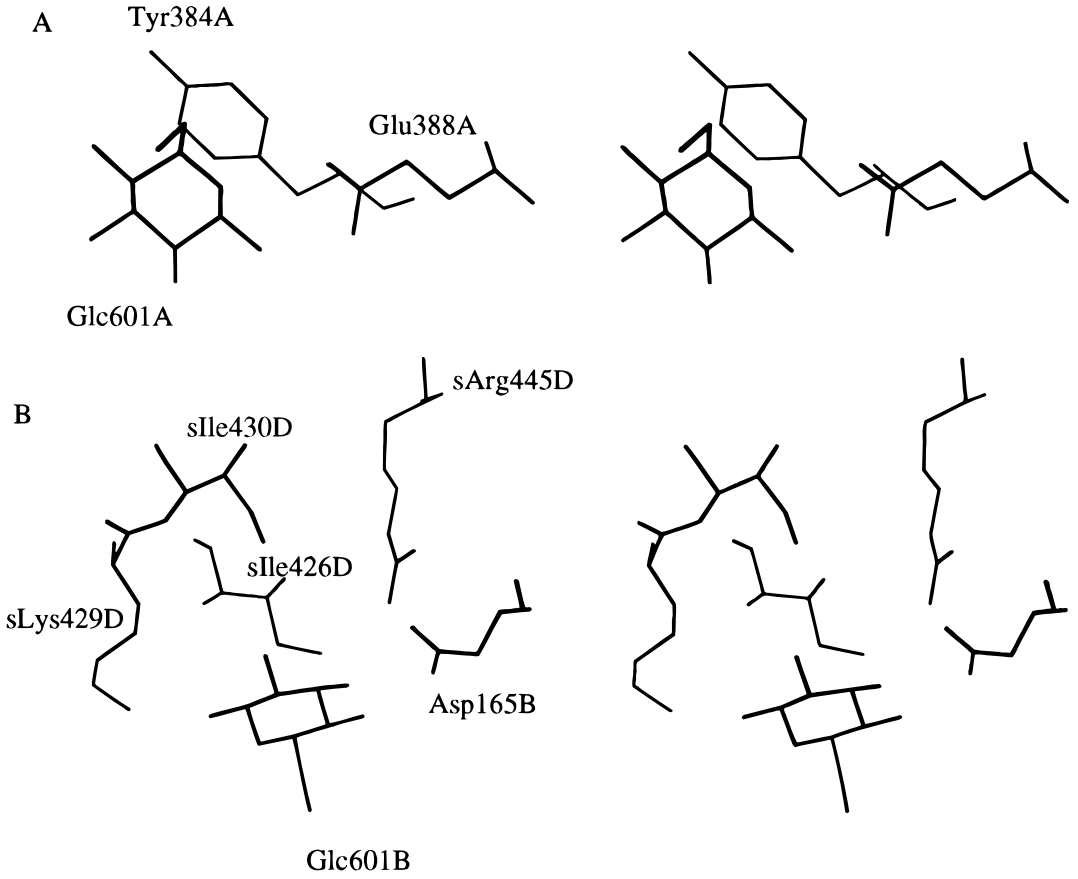

FIGURE 9: Stereoview of the two added β-D glucose molecules. (A) Glc601A and residues within a 5 Å sphere around it. A water involved in hydrogen bonding interactions is not shown. Glu388A is involved in hydrogen bonds to the glucose. (B) Glc601B and residues within a 5 Å sphere around it. Residues from a symmetry-related molecule are signified by an "s" before the residue name. Only Asp165B is involved in hydrogen bonds to the glucose, but side chains of a symmetry-related molecule are nearby.

6.3−6.6 (Yoon et al., 1995). It is not completely clear whether the substrate in the amination direction is ammonia or ammonium ion, and the enzymes from different species may have different substrates (Yoon et al., 1995; Karsten & Viola, 1991; Porter & Bright, 1980). It has been suggested that the enzymatic acid is likely to be uncharged to minimize interference with binding the highly charged substrate (Yoon et al., 1995). Even though the proton to be abstracted has a pK_a higher than 19 (Chiang et al., 1991), the overall rate-determining step of the enzymatic reaction is the cleavage of the carbon−nitrogen bond (Nuiry et al., 1984). Both aspartase and fumarase are thought to use the same chemical mechanism (Porter & Bright, 1980; Blanchard & Cleland, 1980). Fumarase catalyzes the same reaction as aspartase with the final leaving group of the substrate being an -OH rather than an $-NH_3^+$. The two pK_a values for the acid and the base in fumarase are 7.1 and 5.8 (Brant et al., 1963), which are similar to the values in aspartase (Yoon et al., 1995). The determination of the temperature dependence of these pK_a values in fumarase has led to the interpretation that they are caused by an imidazole and a carboxylic acid (Brant et al., 1963).

Despite a careful examination of the structures of aspartase and fumarase, there are still some uncertainties regarding the respective active sites. Conversion of Lys 327 to Arg decreases the aspartase activity to a fraction of a percent of wild-type levels, but there is still detectable activity (Saribas, et al., 1994). The corresponding lysine in fumarase (Lys 324) is also thought to be essential for catalysis (Weaver et al., 1995). Interestingly, in human fumarase, mutation of Glu 315 (fumarase numbering) to Gln abolishes activity. Banaszak and co-workers (Weaver et al., 1995) propose that this Glu is important in the apoenzyme because of a hydrogen bond to a Thr which maintains correct helix positioning. This, in turn, orients another Glu and His properly for a charge relay system which results in the removal of the proton at C3 during catalysis. This charge relay is composed of the same functional groups identified by Alberty and co-workers (Brant et al., 1963), although they are purportedly acting jointly as the base instead of separately as the base and acid. Unfortunately, in *E. coli* aspartase the amino acid corresponding to Glu 315 is already a Gln. Such lack of sequence identity among residues in the active sites of aspartase and fumarase has made it difficult to unambiguously assign the roles of catalytic acid and base. Further discussion of the residues in the active site of aspartase and a comparison with fumarase appears in the following paper.

ACKNOWLEDGMENT

The authors thank Dr. Barry Stoddard (Hutchinson Cancer Research Center, Seattle, WA) for access to an R-axis area detector for data collection and Dr. Len Banaszak (University of Minnesota) for providing a model of fumarase.

REFERENCES

Banaszak, L. J., & Weaver, T. M. (1996) *Biochemistry 35*, 13955−13965.

Beinert, H., & Kennedy, M. C. (1993) *FASEB J. 7*, 1442−1449.
Blanchard, J. S., & Cleland, W. W. (1980) *Biochemistry 19*, 4506−4513.
Brant, D. A., Barnett, L. B., & Alberty, R. A. (1963) *J. Am. Chem. Soc. 85*, 2204−2209.
Brünger, A. T. (1992) *X-PLOR, Version 3.1, A System for X-ray Crystallography and NMR*, Yale University Press, New Haven, CT.
Chiang, Y., Kresge, A. J., Pruszynski, P., Schepp, N. P., & Wirz, J. (1991) *Angew. Chem., Int. Ed. Engl. 30*, 1366−1368.
Chu, S. S. C., & Jeffrey, G. A. (1968) *Acta Crystallogr. B24*, 830−838.
Collaborative Computational Project, Number 4 (1994) *Acta Crystallogr. D50*, 760−763.
Falzone, C. J., Karsten, W. E., Conley, J. D., & Viola, R. E. (1988) *Biochemistry 27*, 9089−9093.
Gewirth, D. (1994) *The HKL Manual*, Yale University, New Haven, CT.
Jayasekera, M. M. K., Shi, W., Farber, G. K., & Viola, R. E. (1997) *Biochemistry 36*, 9145−9150.
Jones, T. A., Zou, J. Y., Cowan, S. W., & Kjeldgaard, M. (1991) *Acta Crystallogr. A47*, 110−119.
Kabsch, W., & Sander, C. (1983) *Biopolymers 22*, 2577−2637.
Karsten, W. E., & Viola, R. E. (1991) *Arch. Biochem. Biophys. 287*, 60−67.
Karsten, W. E., Hunsley, J. R., & Viola, R. E. (1985) *Anal. Biochem. 147*, 336−341.
Kleywegt, G. J., & Jones, T. A. (1993) *CCP4 Newsletter 28*, 56−59.
Kleywegt, G. J., & Brünger, A. T. (1996) *Structure 4*, 897−904.
Kraulis, P. J. (1991) *J. Appl. Crystallogr. 24*, 946−950.
Landro, J. A., Gerlt, J. A., Kozarich, J. W., Koo, C. W., Shah, V. J., Kenyon, G. L., Neidhart, D. J., Fujita, S., & Petsko, G. A. (1994) *Biochemistry 33*, 635−643.
Laskowski, R. A., MacArthur, M. W., Moss, D. S., & Thornton, J. M. (1993) *J. Appl. Crystallogr. 26*, 238−291.
Matthews, B. W. (1968) *J. Mol. Biol. 33*, 491−497.
Navaza, J. (1994) *Acta Crystallogr. A50*, 157−163.
Nuiry, I. I., Hermes, J. D., Weiss, P. M., Chen, C.-Y., & Cook, P. F. (1984) *Biochemistry 23*, 5168−5175.
Porter, D. J. T., & Bright, H. J. (1980) *J. Biol. Chem. 255*, 4772−4780.
Saribas, A. S., Schindler, J. F., & Viola, R. E. (1994) *J. Biol. Chem. 269*, 6313−6319.
Shi, W., Kidd, R., Giorgianni, F., Schindler, J. F., Viola, R. E., & Farber, G. K. (1993) *J. Mol. Biol. 234*, 1248−1249.
Simpson, A., Bateman, O., Driessen, H., Lindley, P., Moss, D., Mylvaganam, S., Narebor, E., & Slingsby, C. (1994) *Nat. Struct. Biol. 1*, 724−734.
Wang, B.-C. (1985) in *Methods in Enzymology* (Wyckoff, H. W., Hirs, C. H. W., & Timasheff, S. N., Ed.) Vol. 115, pp 90−112, Academic Press, Inc., Orlando, FL.
Weaver, T. M., Levitt, D. G., Donnelly, M. I., Wilkens-Stevens, P. P., & Banaszak, L. J. (1995) *Nat. Struct. Biol. 2*, 654−662.
Yoon, M.-Y., Thayer-Cook, K. A., Berdis, A. J., Karsten, W. E., Schnackerz, K. D., & Cook, P. F. (1995) *Arch. Biochem. Biophys. 320*, 115−122.

BI9704515